Supplementary material

Modelling of reabsorption effects

The intensity and spectrum of the fluorescence detected in SPIM depends on several factors:

1. the photon density at the confocal excitation spot.
2. the fluorescence spectrum and quantum yield of the emitting species at the confocal excitation spot
3. the re-absorption of emitted photons by the sample
4. the detection efficiency, which is not expected to vary for detection in different positions in the crystal.

Factors 1 and 4 are both affected by the absorption spectrum of the medium between the microscope objective and the location confocal spot. For a confocal spot at increasing depth in an LHCII crystal, the excitation and detection light travel through an increasingly thick section of LHCII, leading to increased (re-)absorption. This leads to decreased total detected fluorescence, and a red-shift of the fluorescence, because the high-energy (blue) emission photons have a higher probability of being absorbed than red emission photons.

We modelled the spectral dependence on vertical excitation/detection position, by multiplication of the emission spectrum with the transmission spectrum ($T=10^{-\varepsilon(\lambda)cz}$) for a path length of z through the crystal, where c is the concentration of trimeric LHCII in the crystal (2.5 mM[1]) and $\varepsilon(\lambda)$ the wavelength dependent molecular extinction coefficient of the trimeric LHCII. The calculations were done for emission spectra of either trimeric LHCII, aggregates of trimeric LHCII or the spectrum detected by SPIM on the outer edge of the crystal. These all gave very similar results.

Light travelling to and from the focal spot of the objective experiences different path lengths (with different extents of (re-)absorption), due to the high numerical aperture of the objective (1.4). With this numerical aperture the angle under which light travels to/from the focal spot ranges from 0 to ~69°. Different angles contribute to different extents to the total light travelling to/from the focal spot, which was taken into account in the modelling. The final result was convolved with the vertical point spread function.

The modelled spectra are very similar to the experimental spectra (Figure S1). The differences are well within the experimental/modelling uncertainties. The main uncertainties in modelling arise from the unknown refractive index inside the crystal, the uncertainty in the red tail of the absorption spectrum and of the absorption at the excitation wavelength (543 nm), the effect of internal scattering and the uncertainty in the point spread function. From the results in Figure S1, we conclude that within the current precision, the observed spectral dependence on vertical position in the crystal can be completely attributed to (re-)absorption effects. Thus, there are no indications that the fluorescence intensity and spectrum vary vertically in the crystal. This conclusion also holds for excitation at 488 nm and 633 nm, where the main difference is in the lower penetration depth of the excitation light into the crystal.

The spectrum of each voxel of a SPIM dataset was subjected to cubic interpolation. The positions of the maxima of these interpolated spectra are plotted in false-colour in Figure S2, for different horizontal cross-sections of they crystal. There are no indications that the fluorescence intensity and spectrum varies horizontally in the crystal.

From the results in Figures S1 and S2 it can therefore be concluded that the fluorescence spectrum and quantum yield do not vary throughout the crystal. It should be noted that variations smaller that the microscope's psf would be hard to detect.

The total fluorescence of each pixel of data in Fig. S2 was used for a 3D reconstruction (Fig. S3). The crystal has a distinct shape, with tilted surfaces.

The Raman spectra of several crystals were measured in the chlorophyll *b* carbonyl and neoxanthin ν_4 regions. All spectra showed the same characteristic difference with LHCII in detergent buffer. The spectrum of a typical crystal is shown in Figure S4. Most samples also showed strong contributions of free LHCII and/or free pigments present in the crystallization buffer. This presence was also evident from the fluorescence microscopy data (see main text), but there its contribution was readily eliminated by focussing on the crystallized regions only. The contribution of free LHCII/pigments precludes quantitative comparison of the Raman spectra of the different crystal types.

Reference

1 Z. F. Liu, H. Yan, K. Wang, T. Kuang, J. Zhang, L. Gui and W. Chang, *Nature*, 2004, **428**, 287-292.

Supplementary Figures

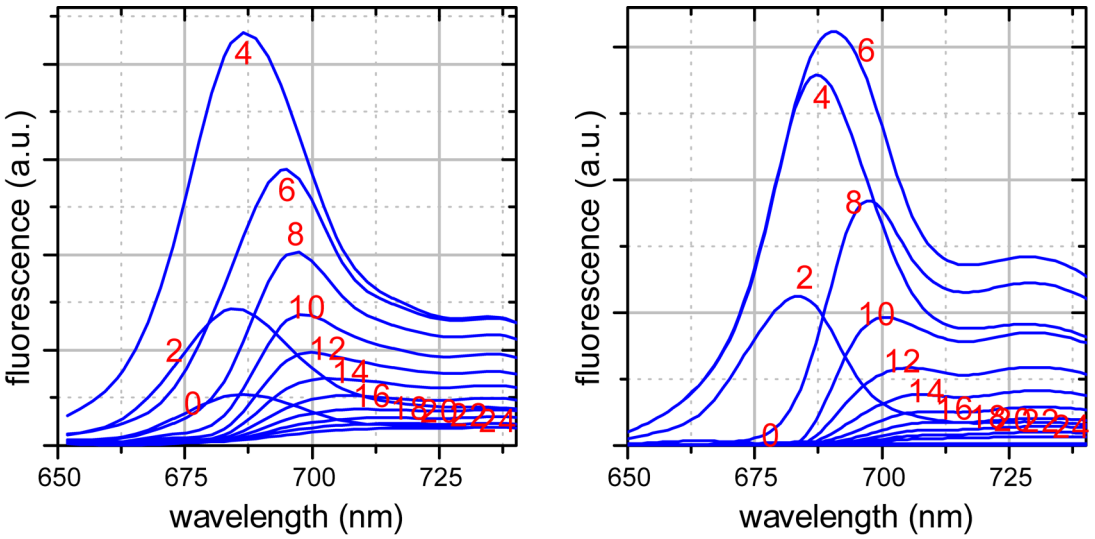

Figure S1 Fluorescence emission spectra detected at different vertical positions in an LHCII crystal (left), and modelled spectra. Vertical positions (in μm) are indicated in red.

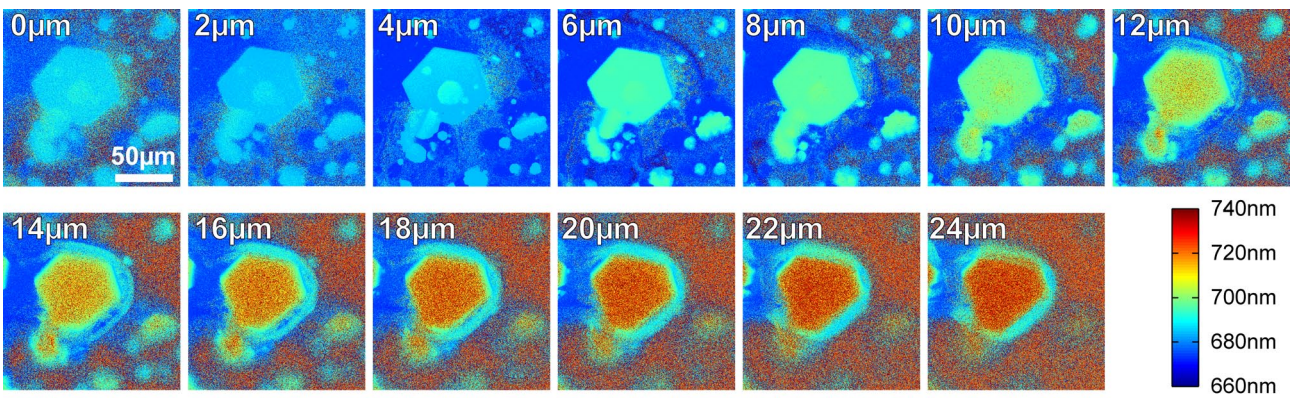

Figure S2 SPIM results of a five-week-old LHCII crystal. False-colour images of the wavelength of maximal emission at different horizontal cross-sections of the crystal. The relative vertical position is indicated in the upper left corner.

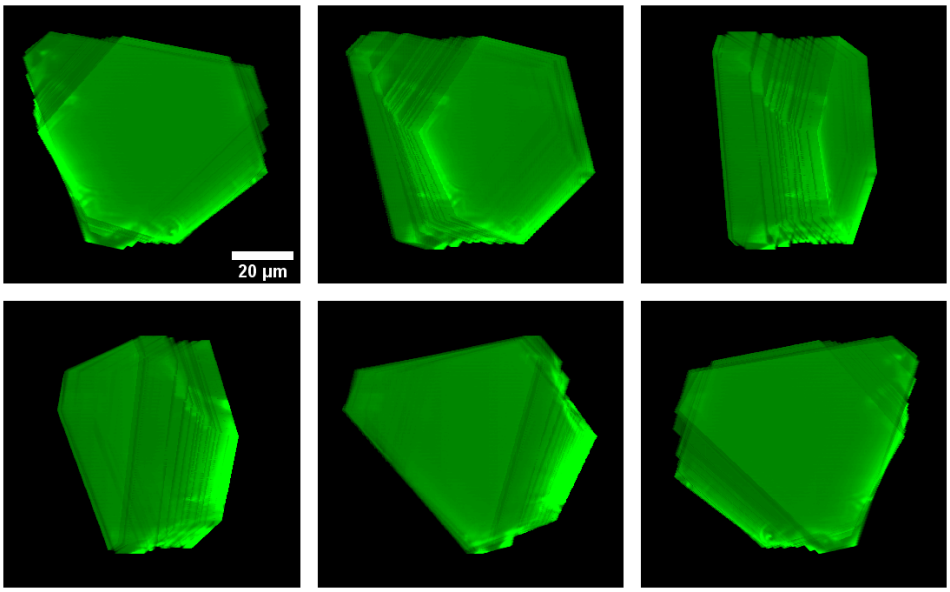

Figure S3 Results of SPIM measurements of one LHCII crystal. Five projections of a 3D reconstruction based on 3D imaging of total chlorophyll fluorescence of the LHCII crystal in Figs. 1 and S1.

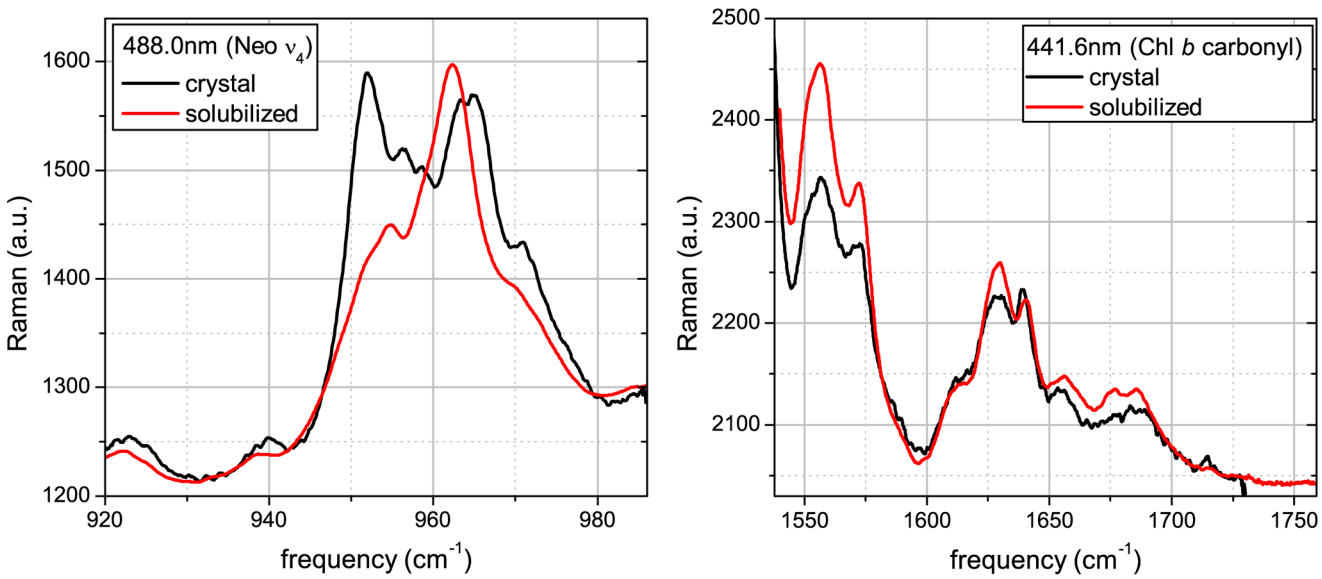

Figure S4 77K Raman spectra of a single LHCII crystal, in the spectral regions of neoxanthin ν_4 (left, excitation at 488.0nm) and Chl *b* carbonyl (right, excitation at 441.6nm).